Please cite this article in press as: Zhang et al., Chiral stacks of a curved nanographene, Chem (2024), https://doi.org/10.1016/j.chempr.2024.07.008

Chem

CellPress
OPEN ACCESS

Article

Chiral stacks of a curved nanographene

Zhongbo Zhang,[1] Dániel Csókás,[2] Israel Fernández,[3] and Mihaiela C. Stuparu[1,4,5,*]

SUMMARY

Despite enormous advances in the edge extension chemistry of nanographenes, examples of *peri*-annulations and the knowledge of their effect on molecular properties remain scarce. Here, we show the synthesis of a curved $C_{60}S_5$ nanographene comprising quintuple [5]thiahelicenes arranged in a C_5-symmetric fashion on the zigzag edge (*L*-region) of a bowl-shaped corannulene core. The synthesis is achieved with the help of Stille coupling, alkynyl thiolation, sulfide/aryne cyclization, and direct arylation reactions. The prepared bowl-helix chiral structure absorbs and emits in the visible and near-IR regions. It assembles into persistent molecular bilayer graphene stacks in solution, solid state, and gas phase. The concave cavities of the supramolecular dimers can recognize the convex surfaces of fullerene C_{60} through shape complementarity and π-π stacking interactions in the solid state. A properties comparison with *ortho*-annulated analogs and archetypical nanographenes indicates the superiority of *peri*-annulations in the design of molecular graphenes.

INTRODUCTION

Annulation of aromatic rings to a polycyclic aromatic hydrocarbon core represents a practical strategy toward controlled growth of nanographenes.[1–4] These annulations can occur at the bay-region (concave armchair edges), *K*-region (convex armchair edges), and *L*-region (zigzag edges) of the core molecule. Among these, aromatic area extensions at the bay-region (*ortho*-*ortho*-annulation) and *K*-region (*ortho*-annulation) are ubiquitous.[1–4] Examples of edge extension through the zigzag edge (*peri*-annulation) are comparatively rare.[5–8] Their significance, however, can be gauged by the rylene series, which is accessed upon zigzag edge extension of naphthylenes.[9,10] They are more stable than acenes and exhibit a lower optical band gap in comparison with the fully benzenoid polycyclic aromatic hydrocarbons.[11] Thus, *peri*-annulations constitute an important yet relatively underexplored mechanism for nanographene formation.

Nanographenes are molecular analogs of graphene. Their discrete multilayered structures, analogous to graphene's layered structure, are anticipated to have properties distinct from the monolayer structure.[12,13] Thus, molecularly layered graphenes are receiving increased attention. However, assembling nanographene multilayers is a challenging task. Covalent systems in which a tether links nanographene fragments cannot be considered true multilayers as the linker becomes the critical factor in governing the interactions between the layers and their properties (which is absent in graphene bilayers).[14–18] Non-covalent systems with low stability and a propensity for higher order assembly and aggregation (being non-discrete) also do not represent molecular bilayers. Thus, supramolecular layered structures of nanographenes having a discrete number of layers and stability in solution, as

THE BIGGER PICTURE

Nanographenes are molecularly precise fragments of graphene with excellent optoelectronic properties and potential applications in future technologies. Thus, the design and synthesis of new nanographene molecules is currently a major research endeavor. The main synthetic strategy to achieve this goal relies on the edge extension of small aromatic molecules. The extension chemistry, however, is mostly restricted to *ortho*-annulations (extension of the bay-region and *K*-region). In this work, we show the importance of *peri*-annulations, extension of the zigzag edges, in nanographene research. We show that *peri*-annulations endow a nanographene molecule with superior electronic properties and the capacity to assemble into discrete multilayer carbon nanostructures.

Please cite this article in press as: Zhang et al., Chiral stacks of a curved nanographene, Chem (2024), https://doi.org/10.1016/j.chempr.2024.07.008

established by Tan and coworkers,[19] remains severely restricted to just a few examples.[19–27]

In this work, we establish quintuple *peri*-annulations on a bowl-shaped corannulene core[28–30] and show their remarkable effect on electronic properties and self-assembly behavior. To achieve this, quintuple [5]thiahelicenes are installed on the core fragment in a C_5-symmetric fashion. The resulting bowl-helix chiral structure assembles into a stable bilayer structure in solution, solid state, and gas phase. The assembly can be extended to include four layers of nanographenes upon molecular recognition with fullerene C_{60}. By contrast, similar systems with 5-fold *ortho*-annulations do not exhibit such self-assembling characteristics.[31–34] Furthermore, *peri*-annulations lead to a large red shift in absorption and emission spectra as compared with *ortho*-annulated analogs. A comparison with archetypical planar nanographenes indicates a significantly lower optical band gap for the *peri*-annulated, curved structure.[11] In essence, this work underlines the importance of *peri*-annulations on the structure and properties of molecular graphene materials.

RESULTS AND DISCUSSION

The synthesis of **4** required four synthetic steps (Figure 1). First, a common precursor in corannulene chemistry, *sym*-pentachlorocorannulene[35,36] was subjected to a palladium-catalyzed ethynylation reaction with the help of trimethyltin-substituted trimethylsilylacetylene.[37] The pentakis(trimethylsilylethynyl)corannulene (**1**) was then subjected to the removal of silyl groups with the help of tetrabutylammonium fluoride followed by 5-fold copper-catalyzed thiolation to obtain **2** in an isolated yield of 27% (over two steps).[38] A cyclization between the alkynyl sulfide moieties in compound **2** and aryne precursor 2-bromo-4-*tert*-butyl-6-(trimethylsilyl)phenyl triflate[39] furnished the benzothiophene-substituted corannulene **3** in 18% isolated yield.[40] Finally, intramolecular cyclization through 5-fold palladium-catalyzed direct arylation under microwave conditions yielded compound **4** in an isolated yield of 11%.[41] In the present system, *ortho*-annulation would have led to the formation of a five-membered ring, while *peri*-annulation led to the formation of a six-membered ring. It is likely that a comparatively lower ring-strain during the formation of a six-membered ring resulted in the observed regio-selectivity toward *peri*-annulation. Moreover, replacing **3** with its chloride analog also led to a successful intramolecular cyclization reaction, albeit with a lower isolated yield of **4** (4%). In **4**, the attachment of the benzothiophene moieties to the corannulene core is through flank (*L*-region) bonds. In all the other known corannulene-core quintuple helicenes, the attachment of the helicene fragments to the core takes place through the rim bonds (*K*-region).[31–34]

Considering helical and bowl chirality elements in **4**,[42–46] sixteen stereoisomers consisting of eight pairs of enantiomers can be envisioned (Figures 2 and S1). To describe these, Figure 2A depicts the nomenclature rules that are inspired by the earlier work from Petrukhina, albeit with the addition of letters ***X*** and ***V*** to clearly distinguish between bowl chirality element from the helical-chirality (which is defined by letters ***P*** and ***M***).[47] Single crystals could be obtained readily to shed more light on these aspects with the help of X-ray crystallography. In a unit cell, we observed two types of diastereomeric monomers, each consisting of one enantiomer pair, namely [***V,MMMMM***], [***X,PPPPP***], and [***V,PPPPP***], [***X,MMMMM***] (Figure 3). However, each enantiomer displayed two distinct conformations distinguished by characteristic torsional angles and bowl depths, which is likely due to the particular intermolecular interactions within the crystal lattice (Figures S2–S5; Tables S1–S5). Thus, the monomers [***V,MMMMM***]—[***X,PPPPP***] and

[1]School of Chemistry, Chemical Engineering and Biotechnology, Nanyang Technological University, 21 Nanyang Link, 637371 Singapore, Singapore

[2]Institute of Organic Chemistry, HUN-REN Research Centre for Natural Sciences, Magyar tudósok körútja 2, 1117 Budapest, Hungary

[3]Departamento de Química Orgánica I, Centro de Innovación en Química Avanzada (ORFEO-CINQA), Facultad de Ciencias Químicas, Universidad Complutense de Madrid, 28040 Madrid, Spain

[4]National Institute for Research and Development of Isotopic and Molecular Technologies—INCDTIM, 67-103 Donat Street, 400293 Cluj-Napoca, Romania

[5]Lead contact

*Correspondence: mstuparu@ntu.edu.sg

https://doi.org/10.1016/j.chempr.2024.07.008

Please cite this article in press as: Zhang et al., Chiral stacks of a curved nanographene, Chem (2024), https://doi.org/10.1016/j.chempr.2024.07.008

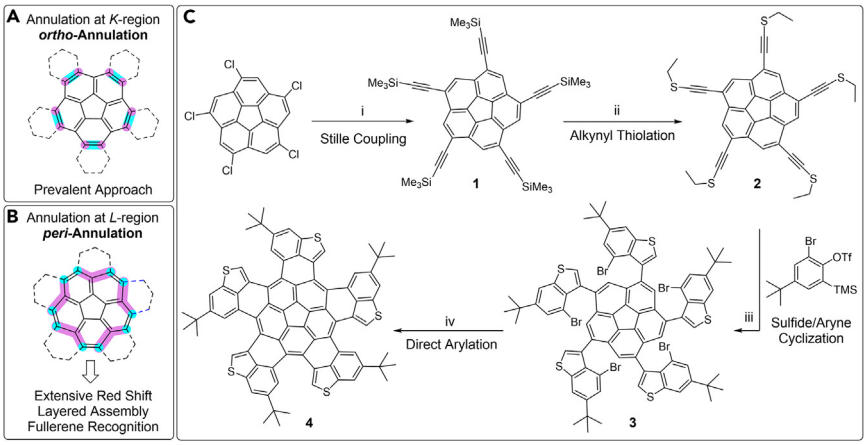

Figure 1. Annulation chemistries on a corannulene core and synthesis of 4

(A) Annulation at *K*-region typically used in the synthesis of curved nanographenes.

(B) Quintuple *peri*-annulations on the zigzag edge of corannulene as established in this work.

(C) Reagents and conditions. (i) Trimethyl((trimethylstannyl)ethynyl)silane (8.0 equiv), $Pd(OAc)_2$ (0.5 equiv), *t*-BuOK (1.0 equiv), IPr·HCl (1.0 equiv), DME, 110°C, 3 days. (ii) *n*-Bu_4NF (10.0 equiv), THF, rt, 1 h; *S*-ethyl 4-methylbenzenesulfonothioate (15.0 equiv), CuI (0.60 equiv), Xantphos (0.72 equiv), K_2CO_3 (7.5 equiv), DMSO, RT, 3 days. (iii) 2-Bromo-4-(*tert*-butyl)-6-(trimethylsilyl)phenyl trifluoromethanesulfonate (60.0 equiv), CsF (90.0 equiv), DME/MeCN, 80°C, 7 days. (iv) $Pd(MeCN)_2Cl_2$ (5.0 equiv), PPh_3 (2.5 equiv), DBN, MeCN, 170°C, microwave, 1 h. Abbreviations: THF, tetrahydrofuran; DMSO, dimethylsulfoxide; DME, dimethoxyethane; DBN, 1,5-diazabicyclo [4.3.0]non-5-ene; MeCN, acetonitrile.

[*V,PPPPP*]—[*X,MMMMM*] are two sets of enantiomer pairs, and the notations **I** and **II** represent the two distinct conformations observed in the crystal structure. Therefore, the molecules identified in the solid state are [*V,MMMMM*]-**I**, [*X,PPPPP*]-**I**, [*V,PPPPP*]-**I**, [*X,MMMMM*]-**I**, [*V,MMMMM*]-**II**, [*X,PPPPP*]-**II**, [*V,PPPPP*]-**II**, and [*X,MMMMM*]-**II**. The eight molecules combined to form four dimers in total, which can be classified into two diastereomeric groups: [*X,MMMMM*]-**I**⊂[*X,PPPPP*]-**I**, [*V,PPPPP*]-**I**⊂[*V,MMMMM*]-**I**, [*X,MMMMM*]-**II**⊂[*X,PPPPP*]-**II**, and [*V,PPPPP*]-**II**⊂[*V,MMMMM*]-**II**. Dimers [*X,MMMMM*]-**I**⊂[*X,PPPPP*]-**I** and [*V,PPPPP*]-**I**⊂[*V,MMMMM*]-**I** showed π-π distance of 3.65 Å. Whereas dimers [*X,MMMMM*]-**II**⊂[*X,PPPPP*]-**II** and [*V,PPPPP*]-**II**⊂[*V,MMMMM*]-**II** showed π-π distance of 3.69 Å. These dimers are packed in two-dimensional (2D) arrays; dimers with ***V***-type of bowls and dimers with ***X***-type of bowls packed in a row by adopting concave-concave and convex-convex packing arrangements, respectively. From the top view of **4**, the radius of its conjugation length is 7.5 Å (Figure S6). From the side view of **4**, the depth of corannulene and its conjugation rim are 0.76 and 2.31 Å, respectively (Figure S6).

Solution studies were then pursued. In ^1H NMR, two sets of proton signals (labeled A and B) with an integral ratio of 1:1 could be observed for **4** at 298 K in deuterated chloroform and benzene (Figures 4A and S7). In deuterated toluene, chlorobenzene, 1,2-dichlorobenzene, and nitrobenzene, three sets of proton resonances (labeled A, B, and C) could be observed with integral ratios of 1:1:0.16, 1:1:0.60, 1:1:1.25, and 1:1:1.46, respectively, at 298 K. In deuterated dichloromethane and tetrachloroethane, the proton resonances sharpen only after decreasing the temperature, thus suggesting a low energy barrier of transition states for interconversion of conformations in these two solvents (Figures S8 and S9). In dichloromethane, integral ratios of 1:1 are observed for A and B at 238 K, whereas in tetrachloroethane, A, B, and C could be observed with an integral ratio of 1:1:0.4 at 258 K. 2D NOESY and ROESY spectra shows intramolecular nuclear

Please cite this article in press as: Zhang et al., Chiral stacks of a curved nanographene, Chem (2024), https://doi.org/10.1016/j.chempr.2024.07.008

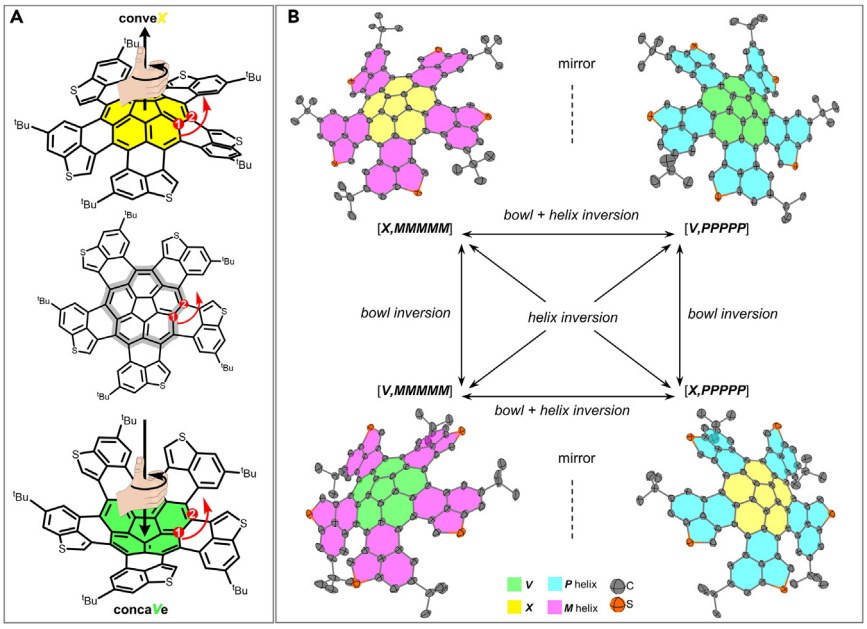

Figure 2. Conformational aspects of 4

(A) Nomenclature of bowl chirality as adopted in this work. Identify the bowl unit and establish priorities as per the Cahn-Ingold-Prelog (CIP) rules (middle). When the fingers of the curled right-hand follow the direction of CIP priority and the thumb points toward the direction of bowl convex, the bowl chirality is defined as ***X*** (top). When the thumb points in the opposite direction of bowl convex, the bowl chirality is defined as ***V*** (bottom).

(B) [***X,MMMMM***] and [***V,PPPPP***] are enantiomers, and [***X,PPPPP***] and [***V,MMMMM***] are enantiomers. These enantiomers can interconvert through bowl and helix inversion processes.

Overhauser effect between different sets of proton signals (A, B, and C), indicating that the molecules are very close in space (≤5 Å) (Figures 5A–5D and S10–S14). Diffusion-ordered spectroscopy (DOSY) showed the same diffusion band for A and B (Figures 5E, 5F, and S15). Proton signals C showed the same diffusion band but a higher diffusion coefficient than A and B. This suggested that signals A and B derive from the species having the same size, whereas signals C result from the species, which has smaller size than A and B. Variable temperature NMR indicated merging and broadening of the signals, indicative of fast conformational changes (helix and bowl inversion) at higher temperatures (>328 K) for chloroform, benzene, toluene, chlorobenzene, 1,2-dichlorobenzene, and nitrobenzene (Figures S16–S21). For variable concentration NMR, in deuterated benzene at 298 K, the integral ratio of signals C increased gradually from less than 3% to over 95% with the concentration decreasing from 5.08×10^{-3} to 8.46×10^{-6} mol/L while the integral ratio of signals A and B remained constant at 1:1 (Figures 4B and S22). In deuterated chloroform at 298 K, the integral ratio of signals C increased gradually from less than 3% to 78% with the concentration decreasing from 5.08×10^{-3} to 8.46×10^{-6} mol/L (Figure S23). Once again, the integral ratio of signals A and B remained constant at 1:1. In deuterated chlorobenzene at 298 K, the integral ratio of signals C increased gradually from 13% to over 95% with the concentration decreasing from 1.52×10^{-2} mol/L (saturated) to 4.23×10^{-5} mol/L, and the integral ratio of signals A and B remained constant at 1:1 (Figure S24).

From these results, it is reasonable to assume that signals A and B are proton resonances of two pairs of C_5-symmetric enantiomers ([***V,PPPPP***] and [***X,MMMMM***]) and ([***X,PPPPP***] and [***V,MMMMM***]) in the dimeric form. Whereas signals C are proton

Please cite this article in press as: Zhang et al., Chiral stacks of a curved nanographene, Chem (2024), https://doi.org/10.1016/j.chempr.2024.07.008

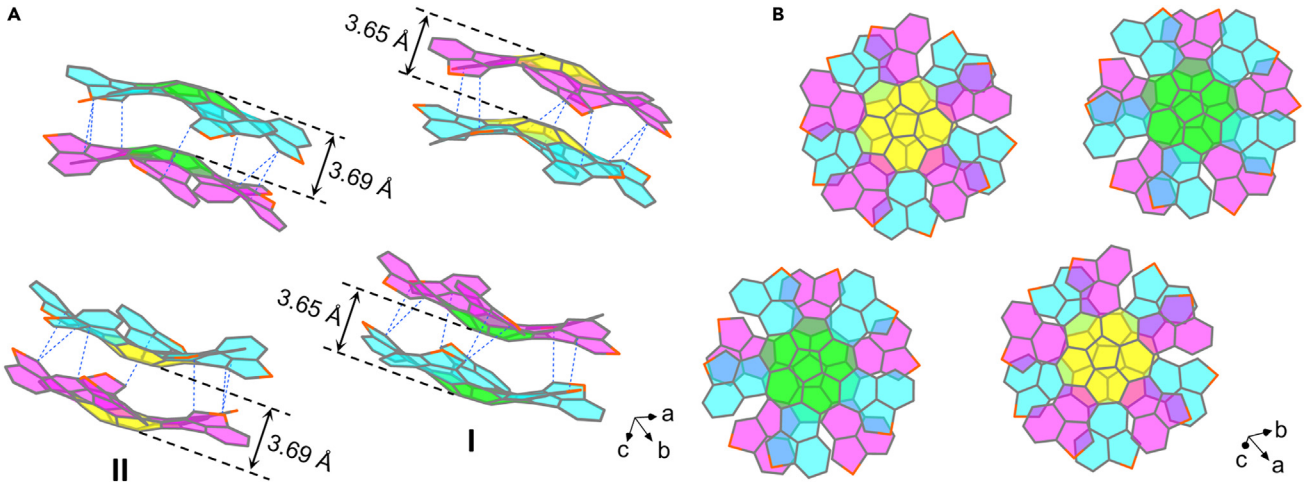

Figure 3. Single crystal structure of 4

tert-Butyl groups, hydrogen atoms, and solvent molecules are omitted for clarity. The π-π distance is defined by the distance between the mean planes of the central five-member rings.

(A) Side view of the molecular packing in the crystalline state of **4**. Aromatic stacking interactions are shown with blue dashed lines.

(B) Top view of the molecular packing in crystalline state of **4**.

resonances of C_5-symmetric enantiomer ([*V,PPPPP*] and [*X,MMMMM*]) in the monomer states. The ratio of signals A and B is always constant in a 1:1 ratio, irrespective of the conditions, and only the content of C is changed upon changing the nature of the solvent and concentration. Solvents of low dielectric constants favor the dimerization even at low concentrations and high temperatures.

Encouraged by the results thus far, high-resolution atmospheric pressure chemical ionization mass spectrometry (HR-APCI-MS) study was carried out. This is a soft ionization technique that hinders molecular fragmentation. This study detected the dimeric species ($[2M+H]^+$) of **4** ($C_{160}H_{121}S_{10}$) at 2,361.6663 in the gas phase and corroborated the solution and solid-state studies in concluding the persistent nature of the supramolecular dimeric species (Figure S25).

Subsequently, fullerene C_{60} was used as a supramolecular glue to bring two bilayers together and form larger nanostructures in the solid state. To this end, co-crystals were grown and studied with the help of X-ray crystallography (Figure 6A).[48,49] In the co-crystals of $\mathbf{4}\subset C_{60}$, eight different molecules of **4** in four conformations like **4** were observed with slight variations in the torsional angles and bowl depths (Figures S26–S29; Tables S6–S10). In the long-range packing of $\mathbf{4}\subset C_{60}$, similar dimers were observed as in the crystal of **4**. One C_{60} molecule coordinated with two dimers, which exhibited the same bowl chirality and formed two types of complexes: complex *X* ([*X,MMMMM*]-I⊂[*X,PPPPP*]-I⊂C_{60}⊃[*X,PPPPP*]-II⊃ [*X,MMMMM*]-II) and complex *V* ([*V,PPPPP*]-I⊂[*V,MMMMM*]-I⊂C_{60}⊃[*V,MMMMM*]-II⊃[*V,PPPPP*]-II), whereas layers of *X* and *V* packed in an alternating fashion in the single crystal.

Variable temperature NMR enabled understanding the thermodynamics of bilayer formation. For this, at a certain temperature and in a certain solvent, the concentration of the monomer and the dimer was determined and converted into the association constant with the help of the equation $K_a = [\mathbf{4}_{dimer}]/[\mathbf{4}_{monomer}]^2$ (Tables S11–S14; Figures S30–S33).[27] These data indicated that the association strength between the two layers is inversely proportional to the dielectric constant of the solvent and the temperature. In chloroform, a solvent that favors dimerization, the association

Please cite this article in press as: Zhang et al., Chiral stacks of a curved nanographene, Chem (2024), https://doi.org/10.1016/j.chempr.2024.07.008

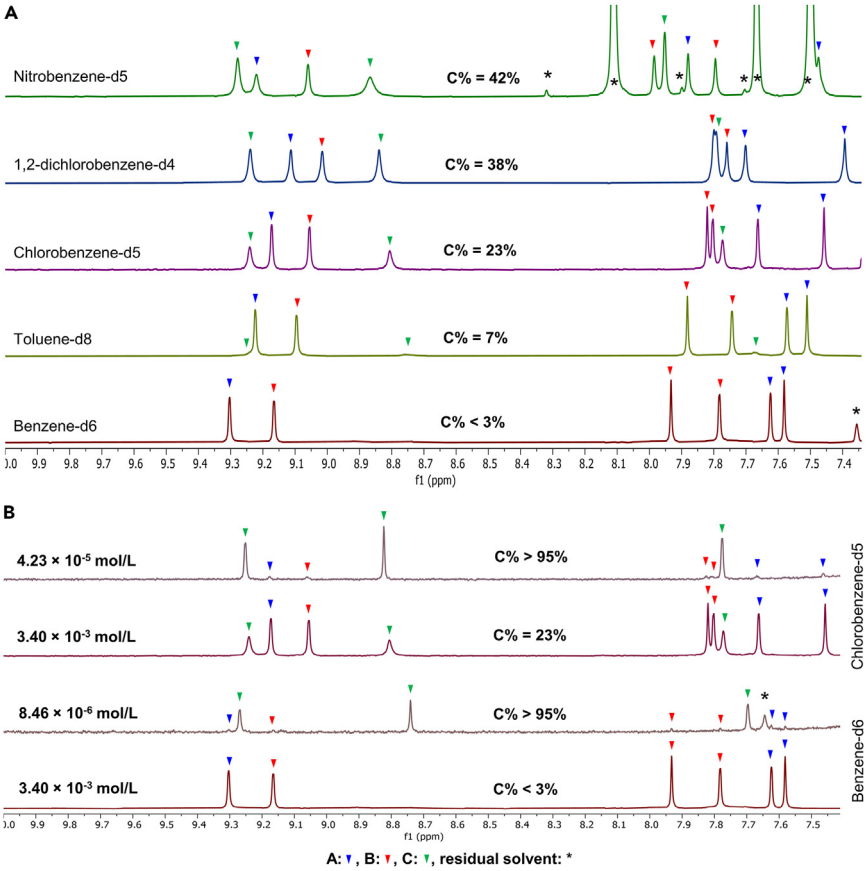

Figure 4. NMR study

(A) Expanded ^{1}H NMR of **4** in different deuterated solvents with a concentration of 3.40 × 10^{-3} mol/L at 298 K.

(B) Expanded variable concentration ^{1}H NMR of **4** in deuterated chlorobenzene (with a concentration of 3.40 × 10^{-3} mol/L and 4.23 × 10^{-5} mol/L) and deuterated benzene (with a concentration of 3.40 × 10^{-3} mol/L and 8.46 × 10^{-6} mol/L) at 298 K.

constant is calculated to be 4.3 × 10^{4} M^{-1} at room temperature. In chlorobenzene, dichlorobenzene, and nitrobenzene, the association constant is calculated to be 1,556, 647, and 319 M^{-1}, respectively, at room temperature. In each solvent, the association constant increased with a lowering of the temperature, and vice versa. A van't Hoff analysis of this data indicated the bilayer formation to be a spontaneous process.

Density functional theory (DFT) calculations were carried out to gain more insights into the conformational (Figures S34–S41) and dimerization aspects (Figures 6B and S42). These calculations helped in quantifying the influence of π-extension and *tert*-butyl-substitution on the stability of the nanographene bilayer. Based on the relative electronic energies, the benzothiophene moieties appear to contribute to the stability of the dimeric form by about 50 kcal/mol, implying that one pair of benzothiophenes increases the stability by 10 kcal/mol. The contribution of *tert*-butyl groups to the dimer stability is comparatively modest as the difference between non-*tert*-butyl-substituted derivative of **4** and dimer of **4** in electronic energy is only ca. 13.0 kcal/mol. This implies that the stability is influenced by approximately 2.6 kcal/mol by each pair of *tert*-butyl groups. These interactions are apparent in the

Please cite this article in press as: Zhang et al., Chiral stacks of a curved nanographene, Chem (2024), https://doi.org/10.1016/j.chempr.2024.07.008

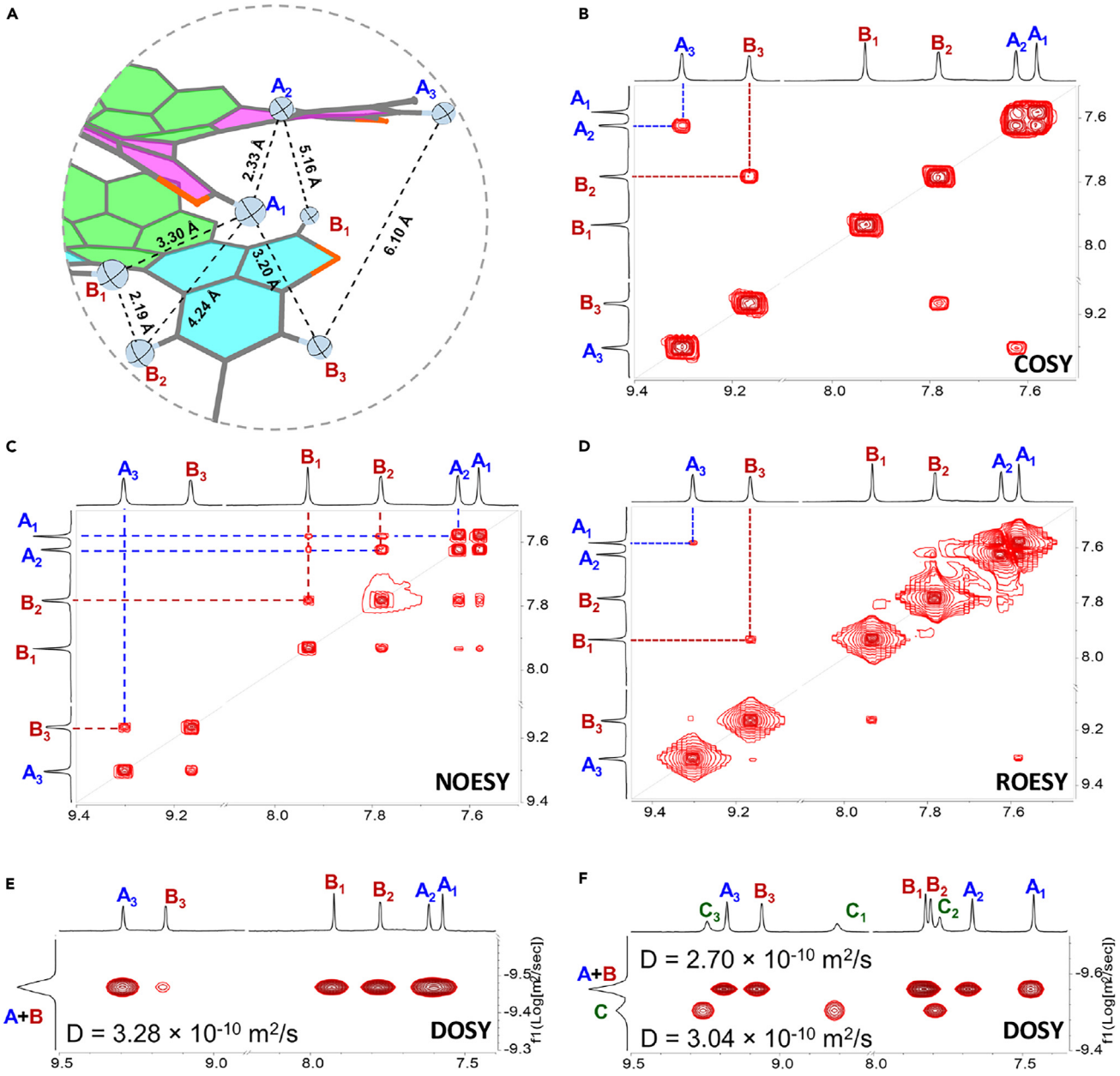

Figure 5. 2D NMR study

(A) Distances among the hydrogen atoms in the molecular bilayer graphene as observed in the crystalline state.

(B) Expanded ^{1}H-^{1}H COSY NMR of **4** in deuterated benzene.

(C) Expanded NOESY NMR of **4** in deuterated benzene.

(D) Expanded ROESY NMR of **4** in deuterated benzene. A concentration of 3.40 × 10^{-3} mol/L at 298 K is used for all experiments.

(E) Diffusion-ordered spectroscopy (DOSY) spectra of **4** in deuterated benzene.

(F) DOSY spectra of **4** in deuterated chlorobenzene. A concentration of 3.40 × 10^{-3} mol/L at 298 K is used for DOSY experiments.

non-covalent interactions (NCIs) plot constructed for the bilayer structure (Figure 6C).[50]

The UV-vis absorption and emission characteristic of **4** was investigated in chlorobenzene at room temperature and at a concentration at which NMR studies (Figure S24) indicate presence of only the monomer (Figures 7 and S43–S45;

Please cite this article in press as: Zhang et al., Chiral stacks of a curved nanographene, Chem (2024), https://doi.org/10.1016/j.chempr.2024.07.008

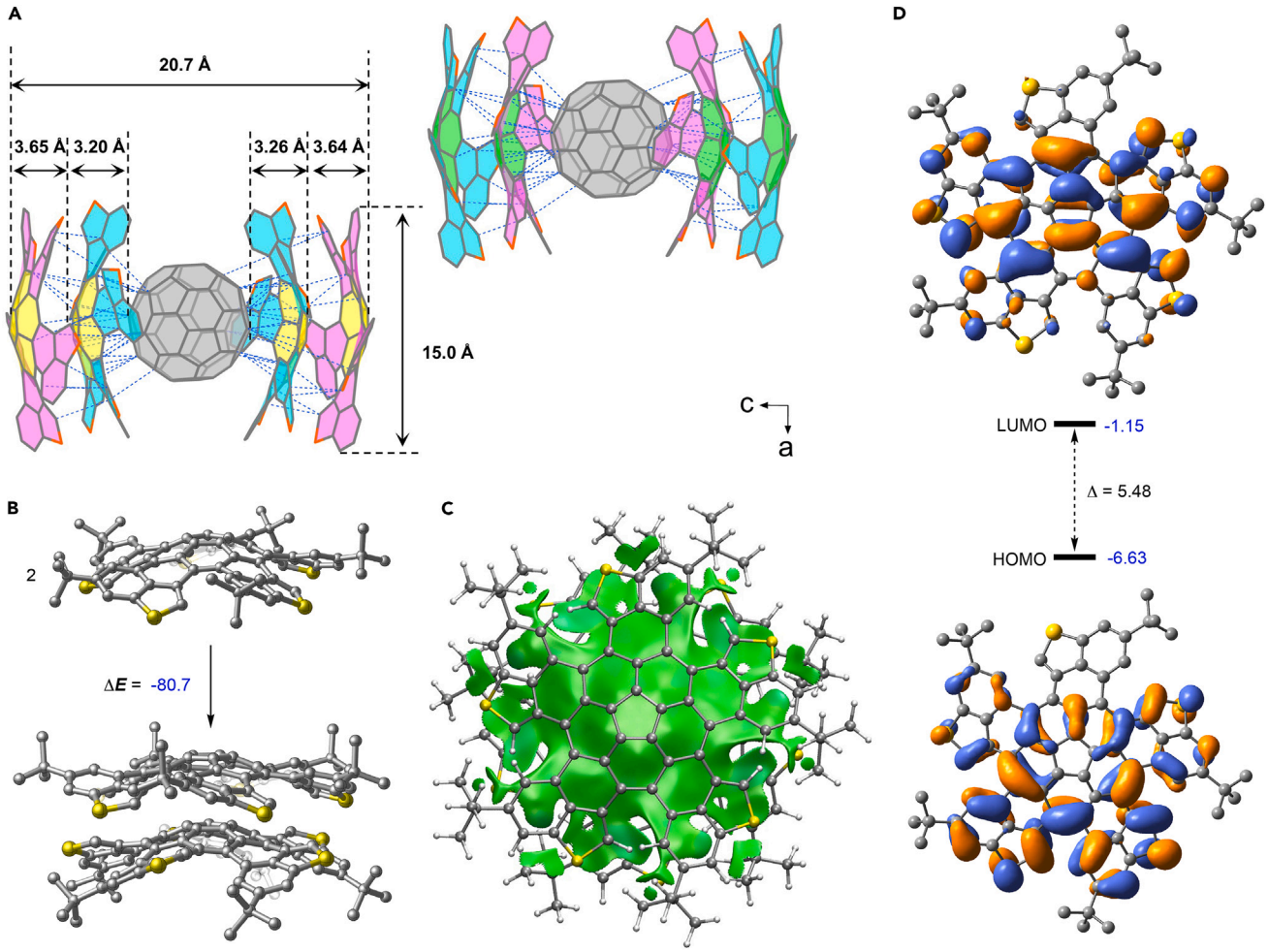

Figure 6. Multilayer assembly of 4 and computational studies

(A) Side view of the molecular packing and aromatic stacking interactions (blue dash lines) of $\mathbf{4} \subset C_{60}$ in single crystalline state. *tert*-Butyl groups, hydrogen atoms, and solvent molecules are omitted for clarity.

(B) Computed energetics of dimerization nanographene **4** and its dimer. The relative electronic energies (ΔE) were calculated at the ωB97X-D/Def2TZVPP level of theory. The ΔE is given in kcal/mol with respect to the most stable monomeric form.

(C) Stabilizing interactions are represented by a green surface in NCI plot of the bilayer structure of **4**.

(D) Frontier molecular orbitals for **4**. Orbital energies (highlighted in blue) and the HOMO-LUMO energy gaps (Δ) are given in eV.

Table S15). The absorption maximum of **4** appears at 573 nm with absorption tailing up to 850 nm. The emission spectrum displays maximum emission at 684 nm with a shoulder at 746 nm. The fluorescence quantum yield is observed to be low ($\Phi \leq 0.1\%$). The optical band gap from the absorption data can be calculated to be 1.79 eV. A comparison can be made to quintuple-helicene systems (**5**–**8**) synthesized through *ortho*-annulation.[31–34] In **7**, nitrogen atoms are directly placed onto the core, which are expected to bring a significant red shift due to their electron-donating character.[33] In **8**, a vast π-system (120 π-electrons) is created with the help of *ortho*-annulation with rylene dyes.[34] Yet, these systems exhibit absorption maxima below 500 nm. A second comparison can be made with archetypical nanographenes **9**–**12**. **9** and **10** contain the same numbers of π-electrons (60) as **4**, while **11** contain a larger number of π-electrons (96).[11] Yet, the optical band gap for **4** is smaller than for **9** (≈2.40 eV), **10** (≈2.19 eV), and **11** (≈1.98 eV). The optical characteristics of **4** are found to be strikingly similar

A

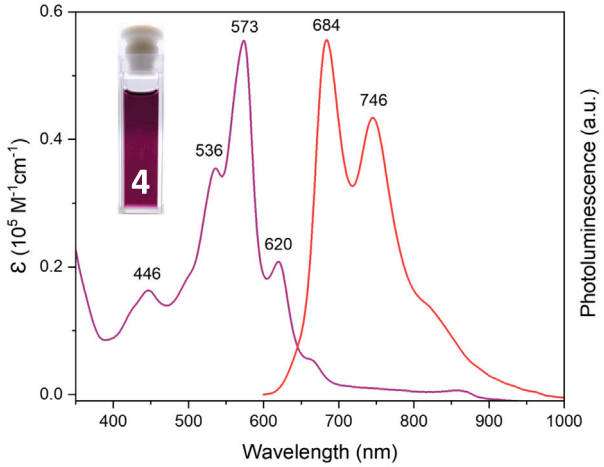

B

Nano-graphene	sp^2-Carbon Atoms	λ_{max} (nm)	Optical Band Gap (eV)
4	60	573	1.79
5	80	385	2.42
6	60	370	2.47
7	70	394	2.52
8	120	480	2.15
9	60	410	2.40
10	60	400	2.19
11	96	460	1.98
12	132	540	1.72

C

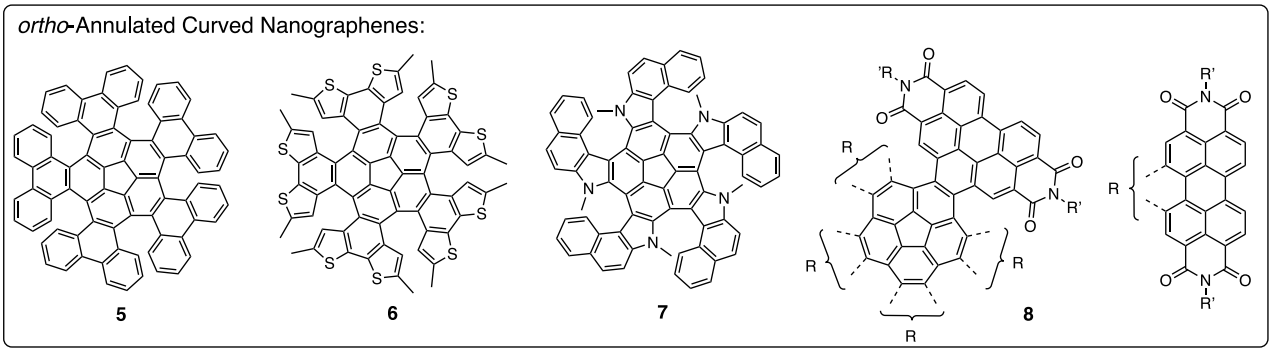

D

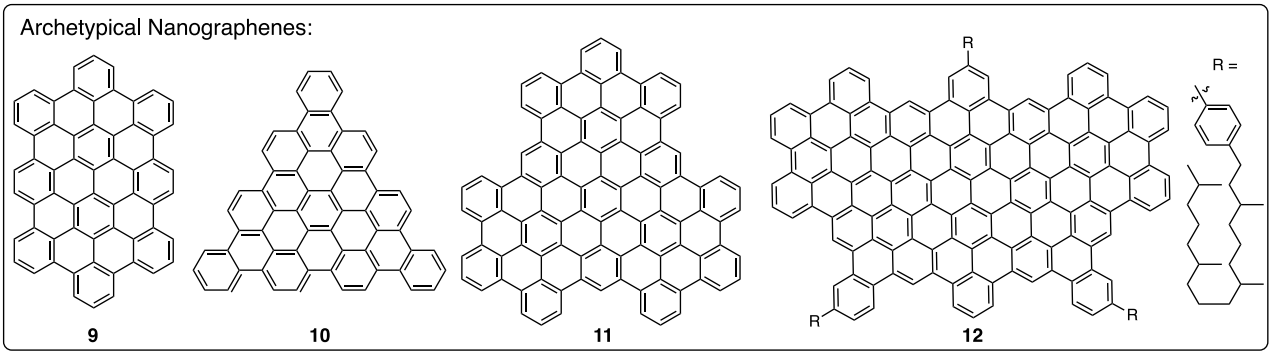

Figure 7. Optical properties comparison

(A) UV-vis absorption (purple line) and fluorescence (red line) spectra of **4** in chlorobenzene at a concentration of 4.23×10^{-6} mol/L along with the digital picture of the solution. Fluorescence spectrum was acquired upon excitation at 400 nm.

(B) Properties of nanographenes **4**–**12**.

(C) Chemical structures of *ortho*-annulated nanographenes.

(D) Chemical structures of archetypical nanographenes.

to an atomically precise graphene quantum dot **12**, which is composed of 2.2 times larger sp^2-carbon atom footprint.[51] While the absorption range is similar, the bands are red shifted in **4**. Interestingly, three long alkyl chains ($C_{20}H_{41}$) are required for the solubilization of **12**. Yet, in comparison with **4**, the vibronic features appear broad, indicating ill-defined aggregation and limited solubility. Overall, this indicates superior electronic properties of **4** over *ortho*-annulated and planar nanographene structures.

Please cite this article in press as: Zhang et al., Chiral stacks of a curved nanographene, Chem (2024), https://doi.org/10.1016/j.chempr.2024.07.008

The electrochemical behavior of **4** was examined by square-wave voltammetry (SWV) and cyclic voltammetry (CV) experiments (Figure S46; Table S16). These results indicated electron-deficient nature of **4** akin to other curved aromatics such as corannulene (which accepts up to 4 electrons) and fullerene C_{60} (which accepts up to 6 electrons). In total, five quasi-reversible reductions were observed for **4**. The first one-electron reduction occurred at −1.75 V versus the ferrocene/ferrocenium couple (Fc/Fc^+). This indicated that 5-fold *peri*-annulations led to a higher electron affinity (with an anodic shift of 0.74 V for the first reduction) than the nanographene core.[52] Finally, the frontier molecular orbital (highest occupied molecular orbital [HOMO] and lowest unoccupied molecular orbital [LUMO]) energies were calculated at the ωB97X-D/Def2TZVPP level (Figure 6D). The HOMO is mainly delocalized through the *peri*-annulated region. By contrast, the LUMO spans across the nanographene core. This is suggestive of a D-π-A character of the overall molecule and likely to be the cause of the observed red shift and the low band gap.[53]

Conclusions

In summary, 5-fold *peri*-annulations on a corannulene core lead to the formation of a bowl-helix hybrid chiral nanographene structure. It exhibits absorption in the 400–850 nm range and fluorescence emission in the 650–900 nm range. In solvents of low dielectric constants, such as chloroform, benzene, and toluene, the nanographene exists as a dimer, which shows stability at millimolar concentrations and temperatures of up to 50°C. The equilibrium can be shifted to monomer in solvents of high dielectric constants, such as chlorobenzene, 1,2-dichlorobenzene, and nitrobenzene, or upon dilution to micromolar concentrations. In the solid state, two pairs of C_5-symmetric enantiomers pack in 2D arrays by adopting concave-concave and convex-convex packing arrangements. A soft ionization technique, HR-APCI-MS, demonstrated the stability of the supramolecular nanographene bilayer in the gas phase. Theoretical calculations indicated dimerization to be unfavorable for the pristine core molecule. Whereas bilayer formation was found to be spontaneous and stabilized mainly by aromatic interactions and aided by dispersion forces in the nanographene structure. Introduction of fullerene C_{60} leads to the formation of host-guest complexes. The fullerene guest is nested in the bilayer nanographene hosts through shape complementarity and π-π stacking interactions. This complex presents a five-layered structure comprising of 300 sp^2-carbon atoms arranged in a 2 × 1.5 nm space. Similar bowl-helix hybrid structures obtained upon *ortho*-annulations neither exhibit long wavelength optical properties nor any tendency to self-assemble into supramolecular structures. A comparison with archetypical nanographenes also indicates a significantly low optical band gap of the present structure. Thus, the work presented here underlines the importance of *peri*-annulations in the synthesis of nanographenes with superior electronic and self-assembling properties. Furthermore, since chiral compounds are known to affect the spins of the electrons passing through them, a phenomenon known as the chiral-induced spin-selectivity effect,[54] the present molecular design, and its possible higher chalcogen variants (selenium and tellurium analogs) may provide interesting bilayer materials for the field of spintronics.

EXPERIMENTAL PROCEDURES

Resource availability

Lead contact

Further information and requests for resources should be directed to and will be fulfilled by the lead contact, Mihaiela C. Stuparu (mstuparu@ntu.edu.sg).

Materials availability

All materials generated in this study are available from the lead contact without restriction.

Data and code availability

The X-ray crystallographic coordinates for structures reported in this study have been deposited at the Cambridge Crystallographic Data Centre (CCDC) under deposition numbers CCDC 2322072 (compound **4**) and CCDC 2322073 (**4**⊂C_{60}). These data can be obtained free of charge from the Cambridge Crystallographic Data Centre via www.ccdc.cam.ac.uk/data_request/cif.

SUPPLEMENTAL INFORMATION

Supplemental information can be found online at https://doi.org/10.1016/j.chempr.2024.07.008.

ACKNOWLEDGMENTS

M.C.S. acknowledges financial support from the Ministry of Education Singapore under the AcRF Tier 2 (MOE-T2EP10221-0002) and funding from the Ministry of Research, Innovation, and Digitalization under Romania's National Recovery and Resilience Plan PNRR-III-C9-2022–I8 program, project code 167/15.11.22. I.F. acknowledges financial support from Spanish MCIN/AEI/10.13039/501100011033 (grants PID2019-106184GB-I00 and PID2022-139318NB-I00). D.C. thanks the Hungarian National Research, Development, and Innovation Office—NKFIH for grant funding (PD-146252). Dr. Li Yongxin is acknowledged for X-ray crystallographic measurements. The authors are grateful to Prof. Li Xinxiong (Fuzhou University) for revising the crystallographic data files.

AUTHOR CONTRIBUTIONS

Z.Z. carried out all the experimental work and prepared data figures. M.C.S. conceived the project and supervised it. D.C. carried out the computational studies relating to monomer conformation, dimerization aspects, and frontier molecular orbitals and described them. D.C., Z.Z., and M.C.S. discussed the association constant studies. I.F. carried out the computational studies related to the NCI plot. M.C.S. prepared the manuscript and revised it with the help of D.C. and Z.Z.

DECLARATION OF INTERESTS

The authors declare no competing interests.

Received: February 12, 2024
Revised: May 11, 2024
Accepted: July 11, 2024
Published: August 12, 2024

REFERENCES

1. Gu, Y., Qiu, Z., and Müllen, K. (2022). Nanographenes and Graphene Nanoribbons as Multitalents of Present and Future Materials Science. J. Am. Chem. Soc. *144*, 11499–11524. https://doi.org/10.1021/jacs.2c02491.

2. Segawa, Y., Ito, H., and Itami, K. (2016). Structurally uniform and atomically precise carbon nanostructures. Nat. Rev. Mater. *1*, 1–14. https://doi.org/10.1038/natrevmats.2015.2.

3. Narita, A., Wang, X.Y., Feng, X., and Müllen, K. (2015). New advances in nanographene chemistry. Chem. Soc. Rev. *44*, 6616–6643. https://doi.org/10.1039/c5cs00183h.

4. Chen, L., Hernandez, Y., Feng, X., and Müllen, K. (2012). From Nanographene and Graphene Nanoribbons to Graphene Sheets: Chemical Synthesis. Angew. Chem. Int. Ed. Engl. *51*, 7640–7654. https://doi.org/10.1002/anie.201201084.

5. Tsvetkov, N.P., Gonzalez-Rodriguez, E., Hughes, A., Dos Passos Gomes, G., White, F.D., Kuriakose, F., and Alabugin, I.V. (2018). Radical Alkyne *peri*-Annulation Reactions for the Synthesis of Functionalized Phenalenes, Benzanthrenes, and Olympicene. Angew. Chem. Int. Ed. Engl. *57*, 3651–3655. https://doi.org/10.1002/anie.201712783.

6. Gonzalez-Rodriguez, E., Abdo, M.A., dos Passos Gomes, G., Ayad, S., White, F.D.,

Tsvetkov, N.P., Hanson, K., and Alabugin, I.V. (2020). Twofold π-Extension of Polyarenes via Double and Triple Radical Alkyne *peri*-Annulations: Radical Cascades Converging on the Same Aromatic Core. J. Am. Chem. Soc. *142*, 8352–8366. https://doi.org/10.1021/jacs.0c01856.

7. Jackson, E.A., Steinberg, B.D., Bancu, M., Wakamiya, A., and Scott, L.T. (2007). Pentaindenocorannulene and tetraindenocorannulene: new aromatic hydrocarbon π systems with curvatures surpassing that of C_{60}. J. Am. Chem. Soc. *129*, 484–485. https://doi.org/10.1021/ja067487h.

8. Lampart, S., Roch, L.M., Dutta, A.K., Wang, Y., Warshamanage, R., Finke, A.D., Linden, A., Baldridge, K.K., and Siegel, J.S. (2016). Pentaindenocorannulene: Properties, Assemblies, and C_{60} Complex. Angew. Chem. Int. Ed. Engl. *55*, 14648–14652. https://doi.org/10.1002/anie.201608337.

9. Markiewicz, J.T., and Wudl, F. (2015). Perylene, Oligorylenes, and Aza-Analogs. ACS Appl. Mater. Interfaces *7*, 28063–28085. https://doi.org/10.1021/acsami.5b02243.

10. Chen, L., Li, C., and Müllen, K. (2014). Beyond perylene diimides: synthesis, assembly and function of higher rylene chromophores. J. Mater. Chem. C *2*, 1938–1956. https://doi.org/10.1039/C3TC32315C.

11. Rieger, R., and Müllen, K. (2010). Forever young: polycyclic aromatic hydrocarbons as model cases for structural and optical studies. J. Phys. Org. Chem. *23*, 315–325. https://doi.org/10.1002/poc.1644.

12. Ohta, T., Bostwick, A., Seyller, T., Horn, K., and Rotenberg, E. (2006). Controlling the Electronic Structure of Bilayer Graphene. Science *313*, 951–954. https://doi.org/10.1126/science.1130681.

13. Zhang, Y., Tang, T.T., Girit, C., Hao, Z., Martin, M.C., Zettl, A., Crommie, M.F., Shen, Y.R., and Wang, F. (2009). Direct observation of a widely tunable bandgap in bilayer graphene. Nature *459*, 820–823.

14. Watson, M.D., Jäckel, F., Severin, N., Rabe, J.P., and Müllen, K. (2004). A Hexa-peri-hexabenzocoronene Cyclophane: An Addition to the Toolbox for Molecular Electronics. J. Am. Chem. Soc. *126*, 1402–1407. https://doi.org/10.1021/ja037520p.

15. Reger, D., Haines, P., Heinemann, F.W., Guldi, D.M., and Jux, N. (2018). Oxa[7]superhelicene: A π-Extended Helical Chromophore Based on Hexa-*peri*-hexabenzocoronenes. Angew. Chem. Int. Ed. Engl. *57*, 5938–5942. https://doi.org/10.1002/anie.201800585.

16. Evans, P.J., Ouyang, J., Favereau, L., Crassous, J., Fernández, I., Perles, J., and Martín, N. (2018). Synthesis of a Helical Bilayer Nanographene. Angew. Chem. Int. Ed. Engl. *57*, 6774–6779. https://doi.org/10.1002/anie.201800798.

17. Reger, D., Haines, P., Amsharov, K.Y., Schmidt, J.A., Ullrich, T., Bönisch, S., Hampel, F., Görling, A., Nelson, J., Jelfs, K.E., et al. (2021). A Family of Superhelicenes: Easily Tunable, Chiral Nanographenes by Merging Helicity with Planar π Systems. Angew. Chem. Int. Ed. *60*, 18073–18081. https://doi.org/10.1002/anie.202103253.

18. Ju, Y.-Y., Chai, L., Li, K., Xing, J.-F., Ma, X.-H., Qiu, Z.-L., Zhao, X.-J., Zhu, J., and Tan, Y.-Z. (2023). Helical Trilayer Nanographenes with Tunable Interlayer Overlaps. J. Am. Chem. Soc. *145*, 2815–2821. https://doi.org/10.1021/jacs.2c08746.

19. Zhao, X.-J., Hou, H., Fan, X.-T., Wang, Y., Liu, Y.-M., Tang, C., Liu, S.-H., Ding, P.-P., Cheng, J., Lin, D.-H., et al. (2019). Molecular bilayer graphene. Nat. Commun. *10*, 3057. https://doi.org/10.1038/s41467-019-11098-9.

20. Hou, H., Zhao, X.-J., Tang, C., Ju, Y.-Y., Deng, Z.-Y., Wang, X.-R., Feng, L.-B., Lin, D.-H., Hou, X., Narita, A., et al. (2020). Synthesis and assembly of extended quintulene. Nat. Commun. *11*, 3976. https://doi.org/10.1038/s41467-020-17691-7.

21. Zhao, X.-J., Hou, H., Ding, P.-P., Deng, Z.-Y., Ju, Y.-Y., Liu, S.-H., Liu, Y.-M., Tang, C., Feng, L.-B., and Tan, Y.-Z. (2020). Molecular defect-containing bilayer graphene exhibiting brightened luminescence. Sci. Adv. *6*, eaay8541. https://doi.org/10.1126/sciadv.aay8541.

22. Mahl, M., Niyas, M.A., Shoyama, K., and Würthner, F. (2022). Multilayer stacks of polycyclic aromatic hydrocarbons. Nat. Chem. *14*, 457–462. https://doi.org/10.1038/s41557-021-00861-5.

23. Pigulski, B., Shoyama, K., Sun, M.J., and Würthner, F. (2022). Fluorescence Enhancement by Supramolecular Sequestration of a C_{54}-Nanographene Trisimide by Hexabenzocoronene. J. Am. Chem. Soc. *144*, 5718–5722. https://doi.org/10.1021/jacs.2c00142.

24. Qiu, Z.L., Cheng, Y., Zeng, Q., Wu, Q., Zhao, X.J., Xie, R.J., Feng, L., Liu, K., and Tan, Y.Z. (2023). Synthesis and Interlayer Assembly of a Graphenic Bowl with Peripheral Selenium Annulation. J. Am. Chem. Soc. *145*, 3289–3293. https://doi.org/10.1021/jacs.2c12401.

25. Niyas, M.A., Shoyama, K., and Würthner, F. (2023). C_{64} Nanographene Tetraimide—A Receptor for Phthalocyanines with Subnanomolar Affinity. Angew. Chem. Int. Ed. Engl. *62*, e202302032. https://doi.org/10.1002/anie.202302032.

26. Jiao, T., Ni, Y., Xu, T., Hou, X., Wu, S., Ren, L., Gu, Y., Miao, X., Sun, Z., and Wu, J. (2023). Synthesis of monolayer and persistent bilayer graphene fragments by using a radical-mediated coupling approach. Nat. Synth. *2*, 1104–1115. https://doi.org/10.1038/s44160-023-00348-w.

27. Ikemoto, K., Kobayashi, R., Sato, S., and Isobe, H. (2017). Synthesis and Bowl-in-Bowl Assembly of a Geodesic Phenylene Bowl. Angew. Chem. Int. Ed. Engl. *56*, 6511–6514. https://doi.org/10.1002/anie.201702063.

28. Tsefrikas, V.M., and Scott, L.T. (2006). Geodesic Polyarenes by Flash Vacuum Pyrolysis. Chem. Rev. *106*, 4868–4884. https://doi.org/10.1021/cr050553y.

29. Wu, Y.-T., and Siegel, J.S. (2006). Aromatic Molecular-Bowl Hydrocarbons: Synthetic Derivatives, Their Structures, and Physical Properties. Chem. Rev. *106*, 4843–4867. https://doi.org/10.1021/cr050554q.

30. Sygula, A. (2011). Chemistry on a Half-Shell: Synthesis and Derivatization of Buckybowls. Eur. J. Org. Chem. *2011*, 1611–1625. https://doi.org/10.1002/ejoc.201001585.

31. Kato, K., Segawa, Y., Scott, L.T., and Itami, K. (2018). A Quintuple [6]Helicene with a Corannulene Core as a C_5-Symmetric Propeller-Shaped π-System. Angew. Chem. Int. Ed. *57*, 1337–1341. https://doi.org/10.1002/anie.201711985.

32. Lin, H.-A., Kato, K., Segawa, Y., Scott, L.T., and Itami, K. (2019). Synthesis and structural features of thiophene-fused analogues of warped nanographene and quintuple helicene. Chem. Sci. *10*, 2326–2330. https://doi.org/10.1039/c8sc04470h.

33. Kise, K., Ooi, S., Saito, H., Yorimitsu, H., Osuka, A., and Tanaka, T. (2022). Five-Fold Symmetric Pentaindolo- and Pentakis(benzoindolo) Corannulenes: Unique Structural Dynamics Derived from the Combination of Helical and Bowl Inversions. Angew. Chem. Int. Ed. Engl. *61*, e202112589. https://doi.org/10.1002/anie.202112589.

34. Meng, D., Liu, G., Xiao, C., Shi, Y., Zhang, L., Jiang, L., Baldridge, K.K., Li, Y., Siegel, J.S., and Wang, Z. (2019). Corannurylene Pentapetalae. J. Am. Chem. Soc. *141*, 5402–5408. https://doi.org/10.1021/jacs.9b00053.

35. Bancu, M., Rai, A.K., Cheng, P., Gilardi, R.D., and Scott, L.T. (2004). Corannulene Polysulfides: Molecular Bowls with Multiple Arms and Flaps. Synlett, 173–176. https://doi.org/10.1055/s-2003-44965.

36. Seiders, T.J., Baldridge, K.K., Elliott, E.L., Grube, G.H., and Siegel, J.S. (1999). Synthesis and Quantum Mechanical Structure of *sym*-Pentamethylcorannulene and Decamethylcorannulene. J. Am. Chem. Soc. *121*, 7439–7440. https://doi.org/10.1021/ja991486q.

37. Wu, Y.-T., Bandera, D., Maag, R., Linden, A., Baldridge, K.K., and Siegel, J.S. (2008). Multiethynyl corannulenes: synthesis, structure, and properties. J. Am. Chem. Soc. *130*, 10729–10739. https://doi.org/10.1021/ja802334n.

38. Kanemoto, K., Yoshida, S., and Hosoya, T. (2019). Synthesis of Alkynyl Sulfides by Copper-Catalyzed Thiolation of Terminal Alkynes Using Thiosulfonates. Org. Lett. *21*, 3172–3177. https://doi.org/10.1021/acs.orglett.9b00875.

39. Ikawa, T., Masuda, S., and Akai, S. (2018). Microflow Fluorinations of Benzynes: Efficient Synthesis of Fluoroaromatic Compounds. Chem. Pharm. Bull. (Tokyo) *66*, 1153–1164. https://doi.org/10.1248/cpb.c18-00578.

40. Matsuzawa, T., Hosoya, T., and Yoshida, S. (2020). One-step synthesis of benzo[*b*]thiophenes by aryne reaction with alkynyl sulfides. Chem. Sci. *11*, 9691–9696. https://doi.org/10.1039/d0sc04450d.

41. Hagui, W., Doucet, H., and Soulé, J.-F. (2019). Application of Palladium-Catalyzed C(sp^2)–H Bond Arylation to the Synthesis of Polycyclic (Hetero)Aromatics. Chem *5*, 2006–2078. https://doi.org/10.1016/j.chempr.2019.06.005.

42. Fujikawa, T., Preda, D.V., Segawa, Y., Itami, K., and Scott, L.T. (2016). Corannulene-Helicene Hybrids: Chiral π-Systems Comprising Both Bowl and Helical Motifs. Org. Lett. *18*, 3992–3995. https://doi.org/10.1021/acs.orglett.6b01801.

43. Yang, W.-W., and Shen, J.-J. (2022). Multiple Heterohelicenes: Synthesis, Properties and Applications. Chemistry *28*, e202202069. https://doi.org/10.1002/chem.202202069.

44. Wu, Y.-F., Zhang, L., Zhang, Q., Xie, S.-Y., and Zheng, L.-S. (2022). Multiple [*n*]helicenes with various aromatic cores. Org. Chem. Front. *9*, 4726–4743. https://doi.org/10.1039/D2QO00988A.

45. Tsurusaki, A., and Kamikawa, K. (2021). Multiple Helicenes Featuring Synthetic Approaches and Molecular Structures. Chem. Lett. *50*, 1913–1932. https://doi.org/10.1246/cl.210409.

46. Kato, K.S., Segawa, Y., and Itami, K. (2019). Symmetric Multiple Carbohelicenes. Synlett *30*, 370–377. https://doi.org/10.1055/s-0037-1610283.

47. Petrukhina, M.A., Andreini, K.W., Peng, L., and Scott, L.T. (2004). Hemibuckminsterfullerene $C_{30}H_{12}$: X-ray Crystal Structures of the Parent Hydrocarbon and of the Two-Dimensional Organometallic Network $[Rh_2(O_2CCF_3)_4]_3 \cdot (C_{30}H_{12})$. Angew. Chem. Int. Ed. *43*, 5477–5481. https://doi.org/10.1002/anie.200460855.

48. Chang, X., Xu, Y., and von Delius, M. (2024). Recent advances in supramolecular fullerene chemistry. Chem. Soc. Rev. *53*, 47–83. https://doi.org/10.1039/d2cs00937d.

49. Sygula, A., Fronczek, F.R., Sygula, R., Rabideau, P.W., and Olmstead, M.M. (2007). A Double Concave Hydrocarbon Buckycatcher. J. Am. Chem. Soc. *129*, 3842–3843. https://doi.org/10.1021/ja070616p.

50. Contreras-García, J., Johnson, E.R., Keinan, S., Chaudret, R., Piquemal, J.-P., Beratan, D.N., and Yang, W. (2011). NCIPLOT: A Program for Plotting Noncovalent Interaction Regions. J. Chem. Theory Comput. *7*, 625–632. https://doi.org/10.1021/ct100641a.

51. Yan, X., Cui, X., and Li, L.-S. (2010). Synthesis of Large, Stable Colloidal Graphene Quantum Dots with Tunable Size. J. Am. Chem. Soc. *132*, 5944–5945. https://doi.org/10.1021/ja1009376.

52. Báti, G., Csókás, D., Giurgi, G.I., Zhou, J., Szolga, L.A., Webster, R.D., and Stuparu, M.C. (2023). Non-Fullerene Electron Acceptors Based on Hybridisation of Corannulene and Thiophene-*S*,*S*-Dioxide Motifs. Chemistry *29*, e202203856. https://doi.org/10.1002/chem.202203856.

53. Xu, Q., Wang, C., Zhao, Y., Zheng, D., Shao, C., Guo, W., Deng, X., Wang, Y., Chen, X., Zhu, J., and Jiang, H. (2020). Tuning the Properties of Corannulene-Based Polycyclic Aromatic Hydrocarbons by Varying the Fusing Positions of Corannulene. Org. Lett. *22*, 7397–7402. https://doi.org/10.1021/acs.orglett.0c02754.

54. Naaman, R., Paltiel, Y., and Waldeck, D.H. (2019). Chiral molecules and the electron spin. Nat. Rev. Chem. *3*, 250–260. https://doi.org/10.1038/s41570-019-0087-1.